Study of the tear topography dynamics using a lateral shearing interferometer

Alfredo Dubra and Carl Paterson
Photonics Group, The Blackett Laboratory, Imperial College London, SW7 2BW, UK
a.dubra@imperial.ac.uk

Christopher Dainty
Applied Optics, Dept. of Experimental Physics, National University of Ireland, Galway, University Road, Galway, Ireland.

http://www.imperial.ac.uk/research/photonics/research/topics/tear_film_topography/index.htm

Abstract: The dynamics of the pre-corneal tear film topography are studied on 21 subjects with a purpose-built lateral shearing interferometer. It was found that in most of the recorded data the tear surface is continuous and smooth. Eye movement is identified as a major problem in quantitative tear topography estimation. Based on the reconstructed tear topography maps, the effects of tear dynamics in visual performance, wavefront sensing for refractive surgery and ophthalmic adaptive optics are discussed in terms of wavefront RMS. The potential of lateral shearing interferometry for clinical applications such as dry eye diagnosis and contact lens performance studies is illustrated by the recorded topography features such as post-blink undulation, break-up, eyelid-produced bumps/ridges, bubbles and rough tear surfaces in front of contact lenses.

OCIS codes: (330.5370) Physiological optics, (010.1080) Adaptive optics, (170.3890) Medical optics instrumentation, (170.4580) Optical diagnostics for medicine, (330.4300) Noninvasive assessment of the visual system and (330.4460) Ophthalmic optics.

References and links

1. H.S. Smirnov, "Measurement of wave aberration in the human eye," Biophys. **6,** 52–66 (1961).
2. I. Iglesias, E. Berrio, and P. Artal, "Estimates of the ocular wave aberration from pairs of double pass retinal images," J. Opt. Soc. Am. A **15**(9), 2466–2476 (1998).
3. J. Liang and D.R. Williams, "Aberrations and retinal image quality of the normal human eye," J. Opt. Soc. Am. A **14**(11), 2873–2883 (1997).
4. T.O. Salmon, L.N. Thibos, and A. Bradley, "Comparison of the eye's wave-front aberration measured psyco-physically and with the Shack-Hartmann wave-front sensor," J. Opt. Soc. Am. A **15**(9), 2457–2465 (1998).
5. W.N. Charman and G. Heron, "Fluctuations in accommodation: a review," Ophthal. Physiol. Opt. **8**(2), 153–164 (1988).
6. L.S. Gray, B. Winn, and B. Gilmartin, "Effect of target luminance on microfluctuations of accommodation," Ophthal. Physiol. Opt. **13**(3), 258–265 (1993).
7. H. Hofer, P. Artal, B. Singer, J.L. Aragón, and D.R. Williams, "Dynamics of the eye's aberration," J. Opt. Soc. Am. A **18**(3), 497–506 (2001).
8. E. Moreno-Barriuso and R. Navarro, "Laser ray tracing versus Hartmann-Shack sensor for measuring optical aberrations in the human eye," J. Opt. Soc. Am. A **17**(6), 974–985 (2000).
9. R. Tutt, A Bradley, C Begley, and L.N. Thibos, "Optical and visual impact of tear break-up in human eyes," Invest. Ophth. Vis. Sci. **41**(13), 4117–4123 (2000).
10. Ignacio Iglesias and Pablo Artal, "High-resolution retinal images obtained by deconvolution from wave-front sensing," Opt. Lett. **25**(24), 1804–1806 (2000).

#5435 - $15.00 US Received 29 October 2004; revised 25 November 2004; accepted 3 December 2004

11. F. Vargas-Martin, P.M. Prieto, and P. Artal, "Correction of the aberrations in the human eye with a liquid-crystal spatial light modulator: limits to its performance," J. Opt. Soc. Am. A **15**(9), 2552–2562 (1998).
12. Shizuka Koh, Naoyuki Maeda, Teruhito Kuroda, Yuichi Hori, Hitoshi Watanabe, Takashi Fujikado, Yasuo Tano, Yoko Hirohara, and Toshifumi Mihashi, "Effect of tear film break-up on higher-order aberrations measured with wavefront sensor," Am. J. Ophthalmol. **134**(1), 115–117 (2002).
13. Luis Diaz-Santana, Cristiano Torti, Ian Munro, Paul Gasson, and Chris Dainty, "Benefit of higher closed-loop bandwidths in ocular adaptive optics," Opt. Express **11**(20), 2597–2605 (2003). http://www.opticsexpress.org/abstract.cfm?URI=OPEX-11-20-2597
14. Nikole L. Himebaugh, Annette R. Wright, Arthur Bradley, Carlolyn G. Begley, and Larry Thibos, "Use of retroillumination to visualize optical aberrations caused by tear film break-up," Optom. Vis. Sci. **80**(1), 69–78 (2003).
15. Xu Cheng, Nikole L. Himebaugh, Pete S. Kollbaum, Larry N. Thibos, and Arthur Bradley, "Test-retest reliability of clinical shack-hartmann measurements," Invest. Ophth. Vis. Sci. **45**(1), 351–360 (2004).
16. M. Glanc, E. Gendron, F. Lacombe, D. Lafaille, J.-F. Le Gargasson, and P. Léna, "Towards wide-field retinal imaging with adaptive optics," Opt. Commun. **230**, 225–238 (2004).
17. T.J. Licznerski, H.T. Kasprzak, and W. Kowalik, "Two interference techniques for in vivo assesment of the tear film stability on a cornea and contact lens," Proc. SPIE **3320**, 183–186 (1998).
18. Alfredo Dubra, Carl Paterson, and J. Christopher Dainty, "Lateral shearing interferometer for the evaluation of tear topography dynamics," To be published in App. Opt. (2004).
19. M. Takeda, H. Ina, and S. Kobayashi, "Fourier-transform method of fringe-pattern analysis for computer based topography and interferometry," J. Opt. Soc. Am. **72**(1), 156–160 (1982).
20. Alfredo Dubra, Carl Paterson, and J. Christopher Dainty, "Wave-front reconstruction from shear phase maps by use of the discrete Fourier transform," App. Opt. **43**(5), 1108–1113 (2004).
21. Austin Roorda, Associate professor, university of houston, college of optometry, houston tx 77204-2020, US. Personal communication," (2002).
22. R. Montés-Micó, J.L. Alió, G. Munoz, and W.N. Charman, "Temporal changes in optical quality of airtear film interface at anterior cornea after blink," Invest. Ophth. Vis. Sci. **45**, 1752–1757 (2004).

1. Introduction

It has been known since Smirnov's work in 1961[1] that the variability in wavefront sensing measurements is dominated not by the wavefront sensors but by changes within the eye. Understanding the sources of this variability is required for making better use of the measurements, for example in the context of refractive surgery. Reported values for the variability of the root-mean-squared (RMS) of the wavefront aberration of the eye are typically $0.1\,\mu$m [1, 2, 3, 4]. An RMS of $0.1\,\mu$m of defocus for a 3mm pupil corresponds to approximately $1/4$ of a diopter (D) , which is the minimum step between consecutive ophthalmic lenses. Therefore, the wavefront aberration variability is not an issue for spectacle prescription. However, when trying to achieve diffraction limited retinal imaging, that is when the RMS of the wavefront aberration of the eye combined with that of the ophthalmic instrument being used has to be kept below Marechal's diffraction limit, $\lambda/14$ (i.e., $0.03-0.05\,\mu$m for visible wavelengths), then the variability of the wavefront sensing measurements is by no means negligible.

Some of the sources of variability in the optical quality of the eye have been identified and characterized, such as the fluctuation of the accommodation [5, 6] whose influence can be reduced by the use of drugs (usually cyclopentolate) [2, 3, 7, 8, 9]. Other sources have been identified but to our knowledge not studied in sufficient depth yet: the eye movement, axial length change [7] and tear dynamics [1, 3, 4, 7, 9, 10, 11, 12, 13, 14, 15, 16].

Most of the research related to the effect of the tear on the optical quality of the eye has so far concentrated on the extreme situation of tear break-up [9, 14]. In 1998, Licznerski *et al.* [17] proposed the use of lateral shearing interferometry for the study of the tear topography, and recently based on this work, we proposed and tested an improved version of this interferometer (and data processing), which is capable of estimating tear topography maps from pairs of lateral shearing interferograms [18]. In this work we present the results of using this interferometer on 21 different subjects, three of them being contact lens users and one with dry eye condition.

#5435 - $15.00 US Received 29 October 2004; revised 25 November 2004; accepted 3 December 2004

2. Lateral shearing interferometer

In order to study the tear topography dynamics we built an interferometer [18] sketched in Fig. 1, that produces pairs of lateral shearing interferograms from a beam reflected off the front surface of the tear film. The phase maps of these interferograms are, to first order, gradients of the tear topography. Thus the need for two interferograms with shear in different directions for the estimation of a single topography map.

The interferometer consists of an illumination branch and two imaging branches. The illumination branch produces a smooth (ideally uniform) normal illumination over a circular region of the front surface of a subject's pre-corneal tear film approximately 3.5 mm in diameter. Although a larger diameter would have been desirable, technical limitations such as the requirement for large optical elements with high numerical apertures and practical issues such as the need for moderate tolerance to eye movement, restricted the studied area of the tear. The light source is a linearly polarized He-Ne laser ($\lambda = 632.8$ nm) with an output power after a neutral density filter (ND) of around 5μW. In this way the power of the radiation reaching the eye is kept 3000 times below safety limits for exposures of up to 100 s according to the British and European standard for Safety of Laser Products (BS EN 60825-1:1994 with amendments 1, 2 and 3). The laser beam at the output of the laser is expanded and spatially filtered using an afocal system formed by a microscope objective, a lens (L_1^{250}) and a pinhole. After reflection on the polarizing beam splitter (PBS), the beam is focused towards the subject's corneal center of curvature, to achieve normal illumination at the tear surface.

The polarization of the laser and the axis of a quarter-waveplate after the PBS were oriented to direct all the light reflected by the tear back into the imaging branches. The use of this combination of optical elements and polarization control, not only keeps the light levels reaching the eye to a minimum, but also reduce the undesired reflections in the system by two orders of magnitude (with respect to a non-polarizing beam splitter configuration).

The two imaging branches produce 1:1 magnification lateral shearing interferograms of the tear film onto a single CCD camera (Retiga 1300, Qimaging), with horizontal and vertical shear. The 3 dimensional folding of the imaging branches makes it possible to image both interferograms onto a single camera, eliminating the need for a second camera and their synchronization. The key optical elements in the interferogram generation are the glass wedges, each of them producing a pair of beams from the reflections on their front and back surface. The tilt between the surface of the wedges leads to fringes in the interferograms, which are required for the phase recovery algorithm used in the data processing. The relative intensity of the interferograms was equalized by rotating the input polarization state of both imaging branches using a $\lambda/2$ waveplate.

The recorded interferograms are processed using Takeda's phase recovery method [19].The spectra of the interferograms show a central peak and two (symmetric) side ones. The separation between these peaks is given by the spatial frequency of the tilt fringes. To extract the phase, the spectra are filtered asymmetrically, by masking out the central peak and one of the side peaks, then inverse Fourier transforming and finally retaining only the imaginary part. The separation of the peaks in the Fourier plane determines the maximum spatial frequency unaffected by the filter, and thus the minimum size of the tear features to be recovered. Finally from each pair of phase maps corresponding to horizontal and vertical shearing, a tear topography map is estimated by using a least-squares integrator [20]. A conservative error estimation in the topography maps accounting for different error sources would be 15% [18].

3. Data collection protocol

A bite registration with soft dental wax was made and mounted on a x-y-z translation stage for precise positioning of the subject with respect to the experiment. When the subject was aligned

#5435 - $15.00 US Received 29 October 2004; revised 25 November 2004; accepted 3 December 2004

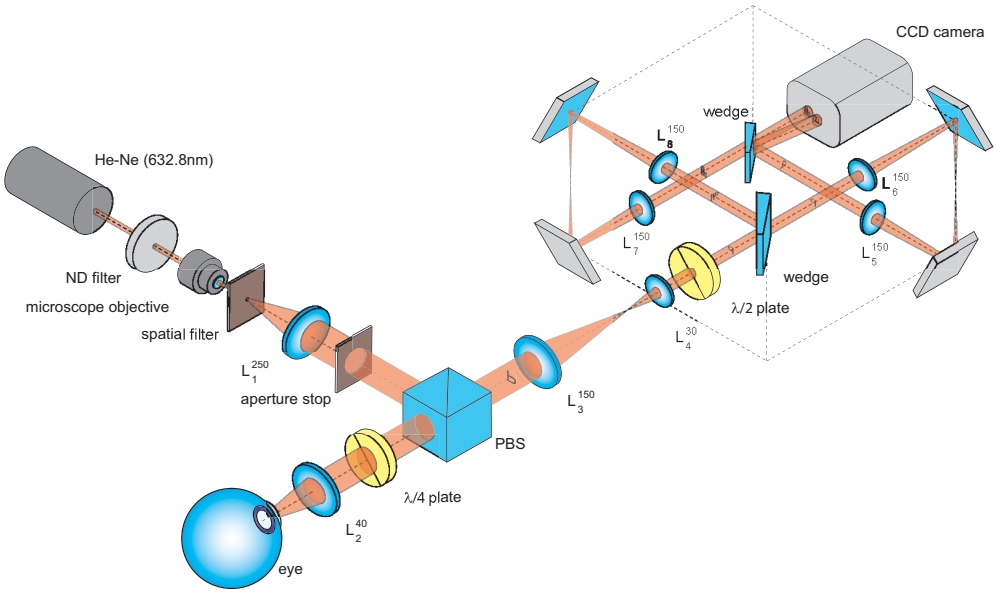

Fig. 1. Sketch of the 3 dimensional lateral shearing interferometer. After the light is reflected back from the front surface of the tear, the first glass wedge produces two horizontally sheared and tilted copies of the incident beam by reflection and a third copy by transmission. The second wedge allows the first pair of copies of the beam to go through unchanged, while on reflection produces a second pair of copies of the beam carrying information from the eye, sheared and tilted in the perpendicular direction. The superscript in the lenses indicates focal length in millimeters.

with respect to the optical system, he/she was asked to remain as steady as possible and to blink normally, while sequences of 100 pairs of shearing interferograms were recorded at a rate of 5 per second. No attempt was made to process the interferograms affected by vignetting, eyelids or eyelashes.

4. Series of raw interferograms

Before performing any data processing, it is worth studying the series of recorded interferograms, where several tear topography features and their evolution can be clearly identified. This suggests that interferometry, and not necessarily lateral shearing interferometry, is potentially a non-invasive clinical tool for tear pathology diagnostics (e.g. dry eye), as illustrated by the movies in Fig. 2. In these movies, the interferograms have been centered to remove most of the eye movement, which otherwise would show the interferograms moving by up to a tenth of the interferogram diameter. The raw sequences consisted of 100 frames, but for display purposes, the frames where the interferograms were vignetted due to large eye movements were removed, hence the discontinuous numbering in some series.

Movie (a) shows a smooth tear surface throughout the approximately 25 s where the subject did not blink. This smooth topography is the most common scenario in the collected data, even when the subjects are not blinking (the average blink rate is approximately 1 every 5 seconds [9]).

Movie (b) shows a sequence with several consecutive blinks. Here it can be seen that the surface is very smooth before the blinks and that immediately after becomes undulated and sometimes even breaks-up (see frame 29/100). This undulation appears in all subjects immediately after

#5435 - $15.00 US Received 29 October 2004; revised 25 November 2004; accepted 3 December 2004

the blink and takes one to two seconds to relax into a smooth surface again.
In movie (c) the tear surface of a regular soft contact lens wearer is shown (without the contact lenses). Throughout the series a number of small tear features with stable positions can be identified. Notice that all of the features are duplicated because the interferogram is formed by overlapping two sheared copies of the same beam. The distance between the duplicated features is the interferogram shear that can be seen at the pupil edge along the horizontal direction. The series of interferograms also shows horizontal bumps/ridges caused by the eyelids, either after reaching and/or resting in a given position and then withdrawing from it. These features are relatively common, and are clearly always horizontal. Some post-blink undulation can also be seen in this series, producing rough surfaces around the small tear features (e.g., frame 13/100).
Movie (d) shows a clear bump/ridge on the top part of the pupil, which moves downwards very slowly until it is flattened during the blink. After the post-blink undulation the surface remains smooth other than for a single small feature (possibly a bubble) that slides downwards until it stabilizes at the center of the pupil.
The series in (e) shows the development of a small tear break-up (top left corner) in an otherwise smooth and very slightly undulated tear surface.
Movie (f) shows the most dramatic surface undulation recorded, ending in the breaking of the tear surface in multiple points, mainly around the pupil edge. It is remarkable how after a single long blink a very smooth continuous tear surface is restored.
In (g) we can see an initially smooth continuous tear surface breaking and undulating before a blink prevents the tear from breaking. Towards the end of the series, the tear eventually breaks simultaneously in several places and the smooth surface is restored after a single blink. This final blink leaves some small features (possibly bubbles) that disappear within half a second (frames 91 and 92/100).
Finally, the movies in (h) and (i) show typical tear surfaces in front of contact lenses, for hard and soft contact lenses respectively. In general the tear surface becomes smoother after blinking, but this does not last. Eventually the surface becomes so rough that fringes cannot be identified. This very high spatial frequency roughness would not change the prescription of the wearer or significantly affect the aberrations of the eye, but more likely increase the scattering.

5. Eye movement and its effect on tear topography measurements

5.1. Eyeball rotation

Let us model the eyeball as a rigid body formed by two spherical surfaces, the sclera with a typical radius of approximately 11 mm and the cornea with 8 mm radius (typical values range from 7 to 9 mm). When the eyeball rotates an angle θ around the center of the sclera (assuming that the center of the corneal surface is 6 mm away from it), the change in observed topography RMS over a circular pupil of 3 mm in diameter is

$$\mathrm{RMS}(\theta) \approx (2.4\,\mu\mathrm{m}) \times \theta. \tag{1}$$

where piston, tip and tilt (which together account for 99.5% of the topography change) were removed, because they do not affect the optical quality of the eye. To convert this topography RMS value to wavefront error RMS in full wavefront sensing measurements in the eye, one only needs to multiply the topography RMS by the difference in refractive indices between air and cornea ($n_{\mathrm{cornea}} \approx 1.37$).

We estimated the movement of the eye by tracking the movement of the center of the recorded interferograms. Figure 3 a shows a typical eye movement pattern over a period of 30 seconds. From the standard deviation of the eye movement (see Figs. 3(b) and (c)) and using formula 1, one can estimate the RMS of the wavefront error that would be produced by eye movement

#5435 - $15.00 US Received 29 October 2004; revised 25 November 2004; accepted 3 December 2004

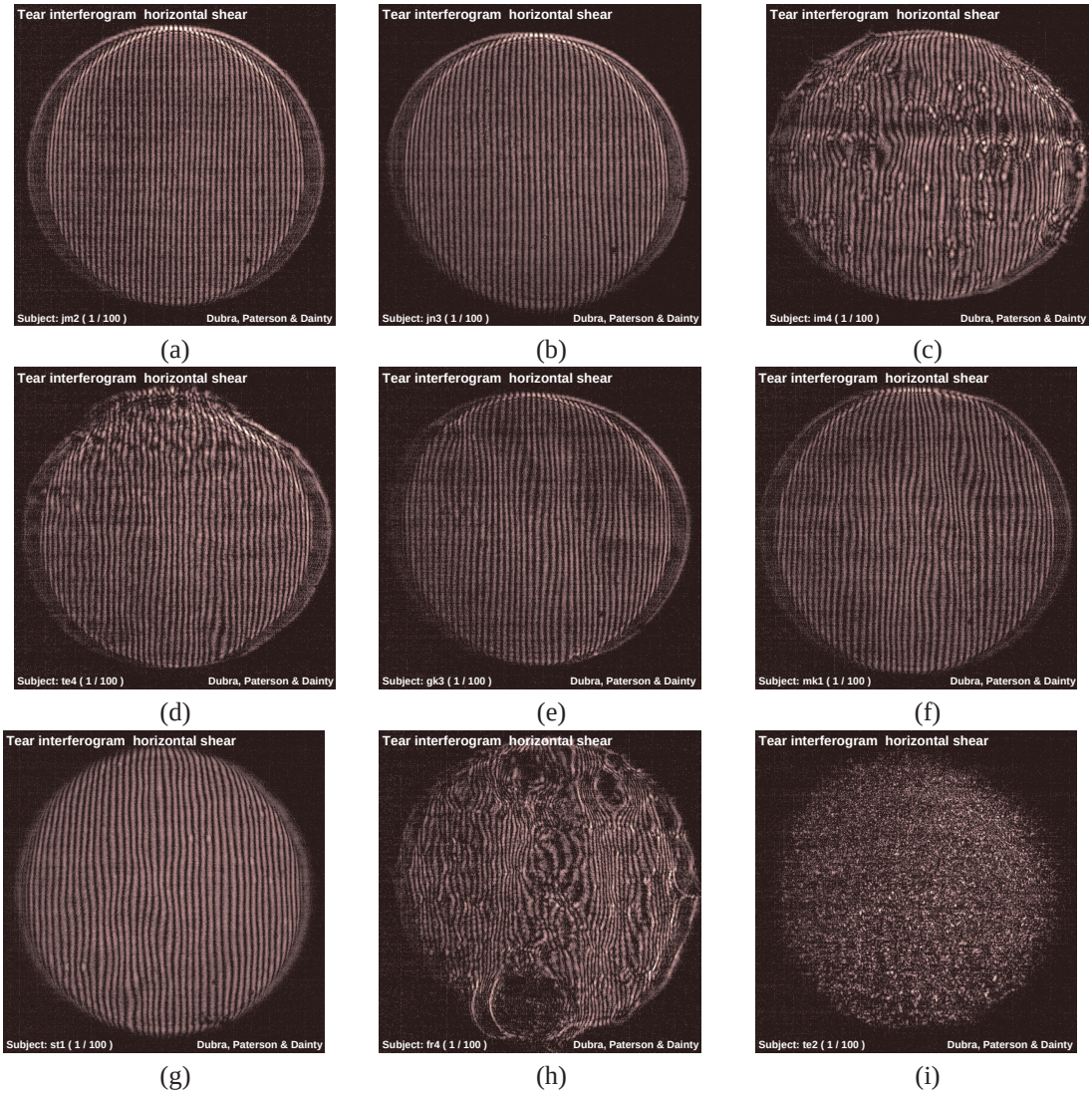

Fig. 2. Movies illustrating tear topography features: (a) smooth surface (2.8MB); (b) post-blink undulation (2.8MB); (c) bubbles and post-blink undulation (2.8MB); (d) eyelid-produced bumps (2.8MB); (e) break-up in an otherwise smooth surface (2.8MB); (f) and (g) dramatic break-up (2.8MB); (h) and (i) rough surfaces in front of hard and soft contact lenses respectively(2.8MB). These movies play at 5 frames per second, that is the rate at which the interferograms were recorded.

of those amplitudes. This can be taken as an estimation of the uncertainty in RMS due to eye movement, giving approximately 0.01μm. This value is too small to explain the large rapid fluctuations of defocus and astigmatism that were measured in the experiments (see plot c in Fig. 6).

#5435 - $15.00 US Received 29 October 2004; revised 25 November 2004; accepted 3 December 2004

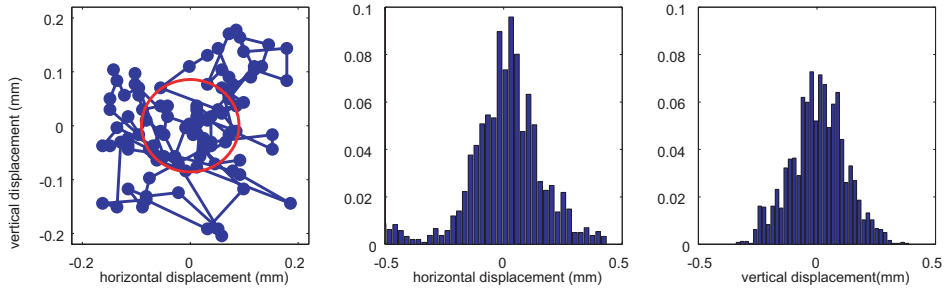

Fig. 3. Eye movement: the plot on the left shows a typical eye movement pattern over 30 s (the radius of the red circle corresponds to one standard deviation); the center and right plots are the normalized histograms of the horizontal and vertical eye displacement for all the 2450 usable frames from 14 different subjects. Both distributions have zero mean and 0.16 and 0.12 mm standard deviations respectively, which is equivalent to 9 nm of wavefront error RMS.

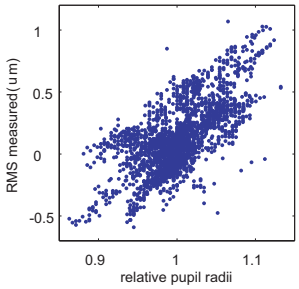

Fig. 4. Correlation between the relative change in the radius of the interferograms and the estimated change in defocus (0.67).

5.2. Head movement

It was noticed in the course of the experiments that despite the use of the bite bar, the head of the subject pivoted a little around the biting point during the 20 to 30 seconds of the data acquisition in a vertical plane. This shows very clearly in the interferograms, as noticeable fluctuations in the interferogram diameter of up to 10 %, and on the number of fringes across the interferograms due to the changes in defocus when the front tear surface changes its distance to the experimental setup along the optical axis. The processed data also shows the head movement through a correlation coefficient of 0.7 between the defocus component of the measured topography maps and the relative change in pupil diameter (Fig. 4). However, by looking at the plots in Fig. 6(c), it seems reasonable to think that the measured fast fluctuations of defocus are not solely due to the much slower head movement (usually with a time scale comparable to that of respiration). We should therefore be aware that both the eyeball rotation and head movement might lead to a small over-estimation of tear topography changes. In order to address this issue, the data analysis considers the tear topography with and without defocus and astigmatism, which are the aberrations introduced by eye movement that have the most impact.

#5435 - $15.00 US Received 29 October 2004; revised 25 November 2004; accepted 3 December 2004

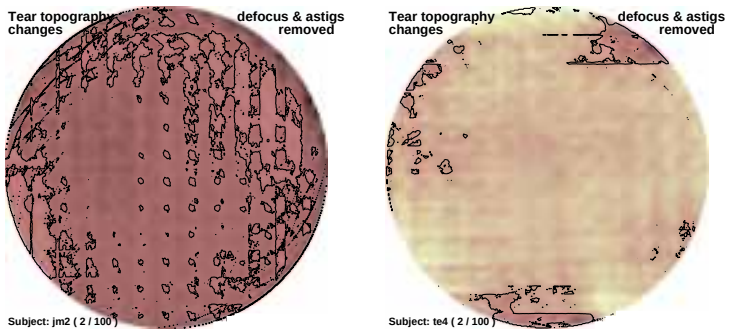

(a) (b)

Fig. 5. Movies of estimated wavefront aberration introduced by the tear topography: (a) corresponds to Fig. 2(a) and shows a very smooth tear surface(4MB);(b) corresponds to Fig. 2(d) and shows the formation and flattening of a bump on the top of the pupil (4MB). The change in wavefront height between consecutive contour lines is $\lambda/14$.

6. Wavefront error RMS introduced by the tear topography

The estimated tear topography maps were converted to wavefront error maps by multiplication by the difference in refractive index between the tear film and air (approximately 0.334).

The movies in Fig. 5 show the wavefront error maps calculated from the series of interferograms in Figs. 2(a) and (d) with defocus and astigmatism removed. The instrument and corneal aberrations were removed by subtracting the first wavefront from the following wavefront maps. In (a) most of the wavefront remains within two contour levels ($\lambda/14$), indicating that in this series, the effect of the tear once defocus and astigmatism are removed is negligible. In (b) the impact of the bump shown in Fig. 2(d) on the wavefront can be seen. Even though the bump is several contour lines deep, the mean RMS of the wavefront throughout the series remains below the diffraction limit (see Fig. 7).

6.1. Wavefront error RMS evolution for individual data series

Figure 6 shows a typical evolution of the wavefront RMS due to tear topography dynamics (relative to the mean wavefront of the series). In all plots, the diffraction limit is indicated as a red line. Plot (a) shows the wavefront RMS of the difference between each wavefront and the mean wavefront of the series. It was found that in all the series of processed data (which correspond to smooth tear surfaces with no break ups) the RMS remains comparable to the diffraction limit. Plot (b) is similar to (a) but the RMS values are calculated from the wavefronts after subtraction of the defocus and astigmatism terms (Zernike polynomials), which are those terms most likely to be significantly affected by eye and head movement. Hereon, we will refer to the wavefront RMS calculated in this way as residual RMS. It was observed that for all the processed data series, these plots are always below the diffraction limit. Finally, plot (c) shows the evolution of the amplitudes of the defocus and astigmatism terms. Here it can be noticed, as in most of the recorded cases, that the defocus term is the dominant aberration in the tear topography dynamics.

6.2. RMS mean values

Let us now look at the wavefront RMS values for all the processed data series, by plotting the mean RMS (brown) and residual RMS (blue) over the data series with more than 75 usable topography maps, corresponding to time intervals of around 30 seconds (see Fig. 7). The

#5435 - $15.00 US Received 29 October 2004; revised 25 November 2004; accepted 3 December 2004

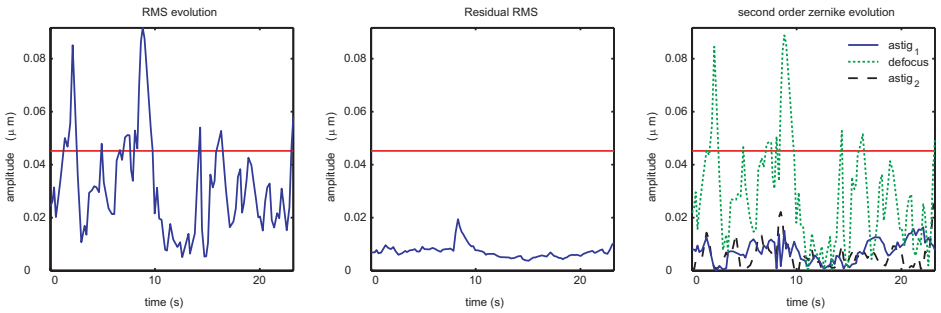

Fig. 6. Typical wavefront RMS evolution due to the tear topography dynamics. The red horizontal line in the plots indicates the diffraction limit for the wavelength used in the experiment. Plot (a) shows the evolution of the RMS (after subtraction of the mean wavefront of the series). Plot (b) is similar to (a) but with the defocus and astigmatism terms removed, and (c) plots the evolution of the defocus and astigmatism components.

numbers on top of the bars are the maximum correlation coefficient between the corresponding RMS and the eyeball rotation and head movement. One can think of these numbers as indicators of the likelihood of the estimated RMS being an artifact due to the undesired eye movements as opposed to true tear topography change.

In almost all cases the mean residual RMS is comparable to or lower than the diffraction limit, while the mean RMS values, including the defocus and astigmatism components seem comparable to or greater than the diffraction limit.

Note that the results shown in Fig. 7 correspond only to a sample of 14 subjects and within those, to the data series with no break-ups or extreme roughness. Thus, it might be argued that Fig. 7 shows an underestimation the RMS values. Nevertheless, the processed data corresponds to the most representative situation (more than 70% of the recorded data series) among non-contact lens wearers.

The analyzed data shows no discernable difference between the tear in front of the contact lenses and the tear in front of the cornea when no contact lens is being worn. However, the analyzed data in this case represents only a small portion (less than 30%) of the recorded data from contact lens users. In the rest of the data, the roughness of the tear surface is such that no fringes could be identified (see Figs. 2(h) and (i)), and therefore no quantitative analysis could be performed.

6.3. RMS mean evolution

We now consider the temporal behavior of the RMS. Figure 8 plots the evolution of estimated RMS (b) and residual RMS (a) for 30 data series , using approximately 2300 topography maps corresponding to 19 different subjects. In this figure, the wavefront RMS deviation has been calculated relative to the first topography map of the series. The residual RMS stays below the

#5435 - $15.00 US Received 29 October 2004; revised 25 November 2004; accepted 3 December 2004

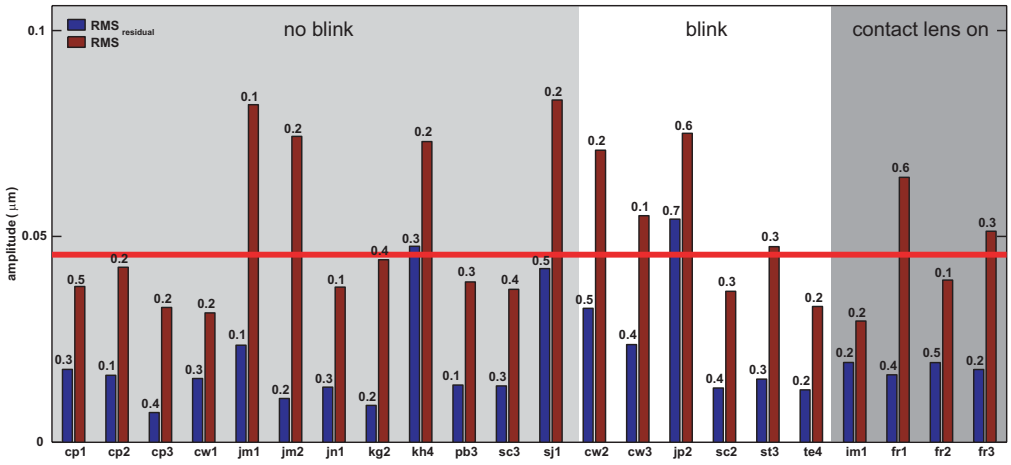

Fig. 7. Mean RMS and residual RMS over the data series corresponding to time intervals of 30 s. The red horizontal line shows the diffraction limit ($\lambda = 632.8$ nm). The data is separated in three groups: on the left (light gray background) are the series in which there were no blinks during the data recording; in the center are series in which there was at least one blink and on the right (dark gray) we show the series in which the subject was wearing contact lenses at the time of the experiment. The numbers on top of the error bars are the the maximum correlation coefficient between the corresponding RMS and the eye and head movement.

diffraction limit even for periods up to 25 seconds (the average blink rate is approximately 1 every 5 seconds [9]). If we now look at the RMS including defocus and astigmatism, we find that (ignoring the eye movement effects), it remains around twice the diffraction limit. This is interesting in the context of wavefront sensing for refractive surgery, because it shows that the effect of the tear topography dynamics is negligible. Defocus with $\lambda/14$ RMS over an 8 mm diameter pupil corresponds to $1/50$ D, which is 25 times smaller that the typical resolution used in spectacles prescription.

However, for adaptive optics for high resolution retinal imaging or psychophysical experiments on individual photoreceptors, even though the degradation of the optical quality of the eye is not very significant, it is by no means negligible. Again, the results obtained here are consistent with Roorda's experience [21] with static wavefront correction on a scanning laser ophthalmoscope (SLO), where he reported some image resolution degradation when trying to resolve photoreceptors after preventing the blink for a few seconds while having accommodation paralyzed.

7. Conclusions

A shearing interferometer for evaluating the dynamics of the front surface of the pre-corneal tear film was tested on 21 subjects. The issue of eye movement, so far ignored in other references [9, 17, 22], is raised and its impact is briefly discussed, noticing that further studies are needed.

The estimated amplitudes of the wavefront RMS introduced by the tear dynamics under normal conditions (i.e., no break-up or contact lenses) are comparable to or smaller than the diffraction limit according to Marechal's criterion, and are consistent with the RMS variability measurements reported for full wavefront sensors in the eye [1, 3, 7, 8]. These results then suggest that the tear topography dynamics under normal conditions does not play a significant

#5435 - $15.00 US Received 29 October 2004; revised 25 November 2004; accepted 3 December 2004

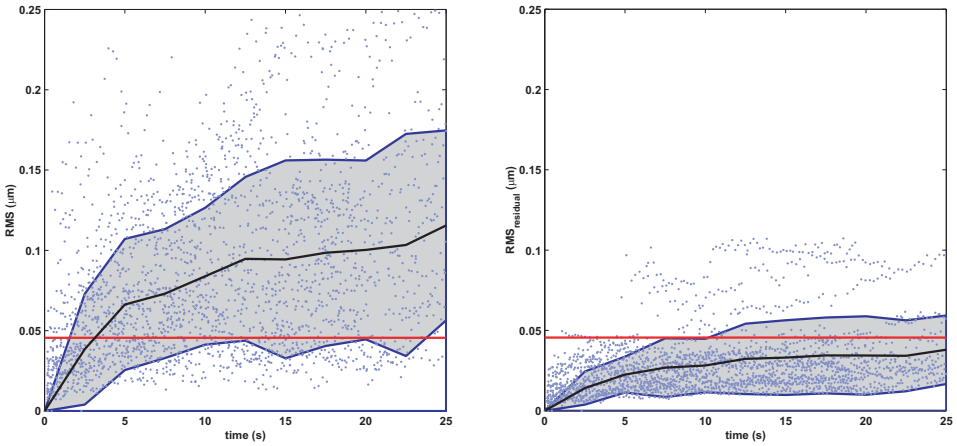

(a) (b)

Fig. 8. Temporal evolution of the estimated wavefront error RMS (a) and residual wavefront error RMS (b) for 30 data series (around 2300 topography maps) corresponding to 19 different subjects. The black lines are the mean RMS at the corresponding time and the gray areas delimited by the blue lines are the areas within one standard deviation from the mean. Again, the red horizontal line indicates the diffraction limit at 632.8 nm.

role in terms of ophthalmic prescription or refractive surgery. In the context of diffraction-limited retinal imaging, the effect of the changes in tear topography are not negligible. If perfect static aberration compensation of the whole eye was applied with some wavefront corrector, such as a deformable mirror, then changes on the tear topography would degrade the image resolution significantly in the scale of seconds.

It was noticed that the front surface of the tear in front of contact lenses is in general very rough, although quantitative analysis of the topography was not possible when the typical roughness was present. We believe this subject should be studied further given the high number of contact lens users.

Finally, it has been shown that lateral shearing interferometry has potential for clinical applications as a non-invasive tool to study the tear topography.

Acknowledgments

This work was supported by the United Kingdom Engineering and Physical Sciences Research Council grant GR R04928-01. Carl Paterson is funded by the Royal Society and Chris Dainty is funded by Science Foundation Ireland under grant number SFI/01/PL2/B039C.

We would like to thank the reviewers for their comments that have greatly improved the manuscript.